ACS OMEGA

http://pubs.acs.org/journal/acsodf

Article

A Superhydrophobic Dual-Mode Film for Energy-Free Radiative Cooling and Solar Heating

Jiang-He Wang, Chao-Hua Xue,* Bing-Ying Liu, Xiao-Jing Guo,* Li-Cui Hu, Hui-Di Wang, and Fu-Quan Deng

Cite This: *ACS Omega* 2022, 7, 15247−15257

Read Online

ACCESS | Metrics & More | Article Recommendations | Supporting Information

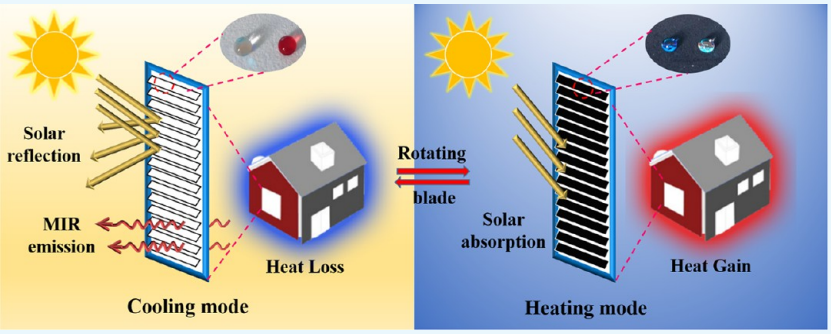

ABSTRACT: Traditional electric cooling in summer and coal heating in winter consume a huge amount of energy and lead to a greenhouse effect. Herein, we developed an energy-free dual-mode superhydrophobic film, which consists of a white side with porous coating of styrene-ethylene-butylene-styrene/SiO_2 for radiative cooling and a black side with nanocomposite coating of carbon nanotubes/polydimethylsiloxane for solar heating. In the cooling mode with the white side, the film achieved a high sunlight reflection of 94% and a strong long-wave infrared emission of 92% in the range of 8−13 μm to contribute to a temperature drop of ∼11 °C. In the heating mode with the black side, the film achieved a high solar absorption of 98% to induce heating to raise the air temperature beneath by ΔT of ∼35.6 °C. Importantly, both sides of the film are superhydrophobic with a contact angle over 165° and a sliding angle near 0°, showing typical self-cleaning effects, which defend the surfaces from outdoor contamination, thus conducive to long-term cooling and heating. This dual-mode film shows great potential in outdoor applications as coverings for both cooling in hot summer and heating in winter without an energy input.

1. INTRODUCTION

Passive daytime radiative cooling (PDRC) has emerged as a highly appealing technique that offered a sustainable way without an additional energy input to cool objects.[1,2] It could simultaneously reflect solar energy in the ultraviolet visible−near infrared (UV−Vis−NIR) wavelength range (0.3−2.5 μm) and send heat into the cold universe through the atmospheric long-wave infrared transparency window (8−13 μm).[3,4] At present, the radiative cooling works reported have basically achieved a good effect that can effectively cool the objects in hot summer.[5−10] However, most of the radiative cooling materials reflect and radiate heat all year round, which saves energy in summer but increases energy consumption in winter.

Therefore, it is significant to realize adaptive heating and cooling in one system to achieve energy saving all year round, including smart windows[11−15] and Janus membranes.[16,17] Kang et al.'s group[18] demonstrated a smart window combining the lower critical solution temperature (LCST) of thermal-responsive polymer hydrogels and the electrical actuation of graphene-based heaters, which modulated thermal energy by transferring from the incident sunlight. When the power was cut off, graphene was cooled and the polymer failed to reach its LCST, where it behaved transparently, allowing light to pass through to heat the object. When powered, graphene was heated and the polymer reached its LCST, where it appeared white and reflected sunlight to cool the object. Zhao et al.[19] proposed a switching strategy based on the dynamic cavitation of silicone coatings that could be tuned from a highly porous state to a transparent solid by stretching and compression. The coating in porous state could reflect light to achieve cooling, while that in transparent solid could allow light to pass through to achieve heating. Hsu et al.[20] demonstrated a dual-mode textile composed of a bilayer emitter embedded inside an infrared-transparent nanoporous polyethylene layer, in which

Received: March 30, 2022
Accepted: April 7, 2022
Published: April 18, 2022

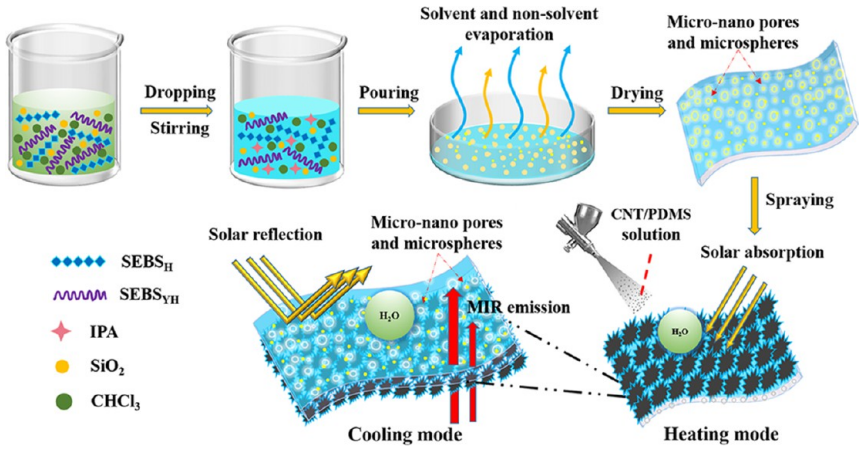

Figure 1. Schematic illustration of the fabrication procedures of the dual-mode film.

the bilayer emitter was made up of a carbon layer and an emitting layer. It achieved heating by facing the low-emissive carbon layer outside and cooling by facing the high-emissive emitting layer outside. These reports have great potentials to save the limited energy reserves and mitigate an urban heat island effect. However, it should be noted that there are only a few works about such materials, which need improvement in heating and cooling performance, and existing materials are limited in their practical application, which require external electricity and extra force to achieve a heat-regulated switch. In addition, these materials are so easily affected by moisture and dust that their reflection and photothermal ability would decrease as time goes on and dust accumulates.[21−29] Therefore, it is necessary to develop an efficient cooling and heating material with a self-cleaning function to remove dust pollutants for long-term outdoor applications.

Here, a superhydrophobic dual-mode film was developed by a nonsolvent-induced phase separation and one-step spray method (Figure 1). The film consisted of a white side with porous coating of styrene-ethylene-butylene-styrene and SiO_2 nanoparticles ($SEBS_{H/YH}/SiO_2$) for radiative cooling and a black side with nanocomposite coating of carbon nanotube/polydimethylsiloxane (CNT/PDMS) for solar heating. Owing to the disordered micro/nanoporous structures of the $SEBS_{H/YH}/SiO_2$ coating in the white side, the film showed a high solar reflectance of 94% and a long-wave infrared emissivity of 92% to contribute to a temperature drop of ∼11 °C. Meanwhile, a high solar absorption of 98% was achieved by the black side of the film due to the photothermal conversion capacity and full absorption of the UV−Vis−NIR spectrum of the CNT/PDMS coating, which induced solar heating to raise the air temperature beneath by ΔT of ∼35.6 °C. Additionally, the micro/nanorough structures and the low surface energy of the cooling and heating surfaces endowed the dual-mode film superhydrophobic self-cleaning properties, which prevented the material from contamination, which thus helped maintain the cooling and heating performance for long-term outdoor applications. Moreover, this dual-mode film was made from commercially available materials via a facile, fast method; therefore, it shows great potentials in many applications.

2. EXPERIMENTAL SECTION

2.1. Materials. The copolymer of styrene-ethylene-butylene-styrene ($SEBS_H$, H1062, S/EB = 18:82) was purchased from Japan Asahi Kasei Co., Ltd. The copolymer of SEBS ($SEBS_{YH}$, YH602, S/EB = 35:65) was obtained from China Petrochemical Group Co., Ltd. Hydrophobic SiO_2 (16 nm) was purchased from Yuanjiang Chemical Co., Ltd. (Shanghai, China). Multiwalled carbon nanotubes (CNTs; purity, 95%; 10−30 nm in diameter) were acquired from Chengdu Organic Chemistry Co., Ltd. The PDMS (Sylgard 184) precursor principal agent and its curing agent were purchased from Dow Corning, USA. Other reagents and solvents like isopropyl alcohol, chloroform, and tetrahydrofuran (THF) were bought from Sinopharm Chemical Reagent Co., Ltd., and used as received.

2.2. Fabrication of the $SEBS_{H/YH}/SiO_2$ Film. $SEBS_H$ and $SEBS_{YH}$ were first dissolved in 30 g of chloroform at a mass ratio of 6:4 to prepare $SEBS_{H/YH}$ solution. Then, 0.02 g of hydrophobic SiO_2 was dispersed in the $SEBS_{H/YH}$ solution under stirring. Next, 8 g of isopropyl alcohol as a nonsolvent was slowly added to the prepared $SEBS_{H/YH}/SiO_2$ dispersion by a peristaltic pump under stirring, followed by sonication for 10 min to form a $SEBS_{H/YH}/SiO_2$ gel. The resulted gel was poured into a culture dish and dried under ambient conditions to complete the phase separation with the surrounding humidity controlled at about 65%. Finally, a $SEBS_{H/YH}/SiO_2$ film with micro/nanopores and microspheres was obtained. For comparison, $SEBS_H$, $SEBS_{YH}$, and $SEBS_{H/YH}$ films without adding SiO_2 were also fabricated using the same phase separation method to serve as control samples.

2.3. Fabrication of the CNT/PDMS-$SEBS_{H/YH}/SiO_2$ Film. A PDMS solution was prepared by dissolving PDMS principal agent and curing agent (mass ratio of 10:1) into THF with PDMS, accounting for 6 wt % THF, and ultrasonicated for 10 min. Afterward, a given amount of CNTs was added to the PDMS solution and ultrasonicated for 20 min with the mass ratio of PDMS to CNT controlled at 2:1 to form a CNT/PDMS solution. Then, the CNT/PDMS solution was spray-coated on the above-fabricated $SEBS_{H/YH}/SiO_2$ film through a stencil mask using an airbrush (G222; Master Airbrush). The spraying process was carried out under ambient conditions with a nozzle to the substrate distance of ∼15 cm and airbrush pressure of ∼20 psi. Finally, the CNT/PDMS-coated $SEBS_{H/YH}/SiO_2$ film was dried at 60 °C for 30 min in air to obtain a CNT/PDMS-$SEBS_{H/YH}/SiO_2$ film.

2.4. Characterization. *2.4.1. Morphology and Wetting States.* The surface and cross-sectional morphologies of the films were measured using field emission scanning electron

https://doi.org/10.1021/acsomega.2c01947
ACS Omega 2022, 7, 15247−15257

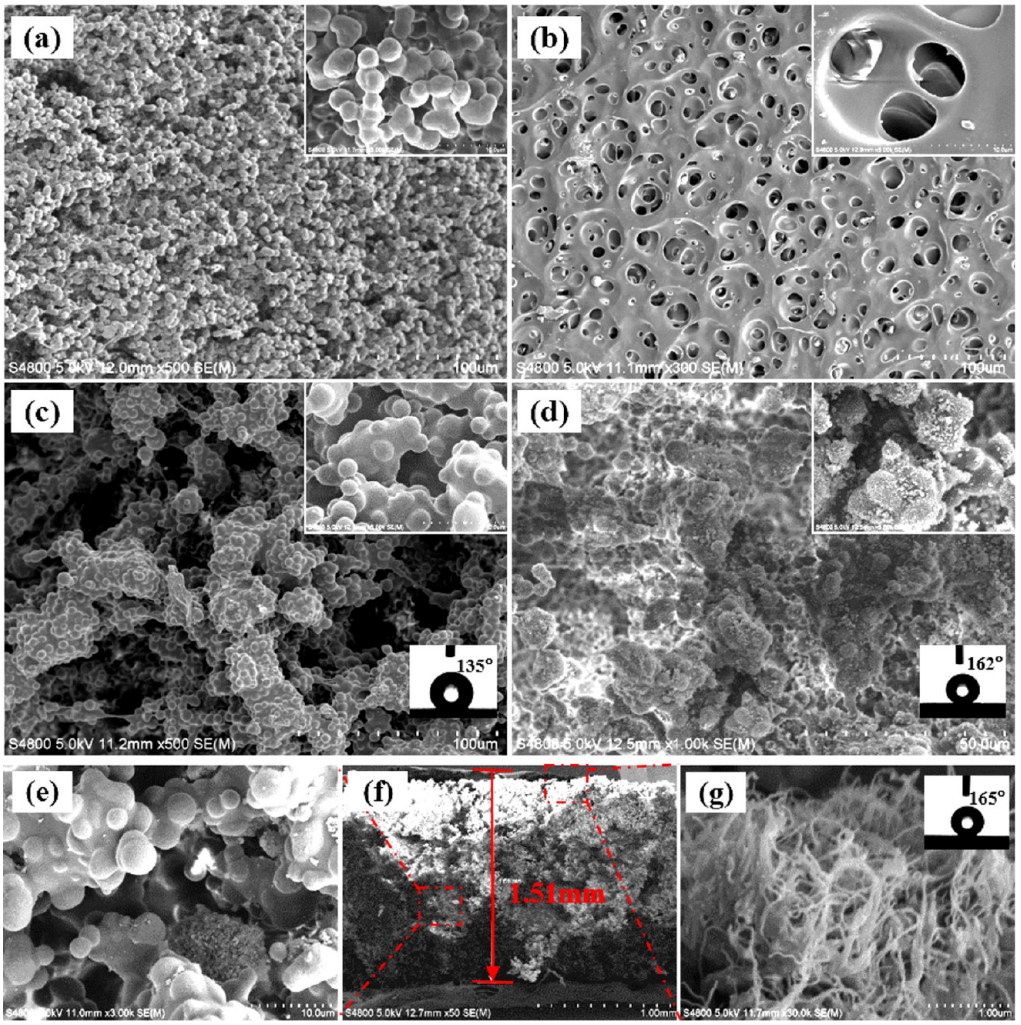

Figure 2. SEM images of (a) $SEBS_H$ film, (b) $SEBS_{YH}$ film, (c) $SEBS_{H/YH}$ film, (d) and $SEBS_{H/YH}/SiO_2$ film; (e) magnification of $SEBS_{H/YH}/SiO_2$ in the cross section of the CNT/PDMS-$SEBS_{H/YH}/SiO_2$ film; (f) cross section of the CNT/PDMS-$SEBS_{H/YH}/SiO_2$ film; (g) magnification of CNT/PDMS at the cross section of the CNT/PDMS-$SEBS_{H/YH}/SiO_2$ film.

microscopy (SEM; Hitachi S-4800). Energy dispersive spectroscopy (EDS) was used to measure the distribution of the elements in the film. Water contact angles (CAs) and sliding angles (SAs) of the sample were measured using a video optical contact angle system (OCA 20, Data Physics, Germany) with 5 and 10 μL of water droplets, respectively. All the values of CA and SA were determined by averaging values measured at five points on each sample.

2.4.2. Optical Characterization. The reflectance of the films was measured separately in the ultraviolet, visible-to-near-infrared (0.3−2.5 μm), and mid-infrared ranges (2.5−25 μm). The first range measurement was taken using an ultraviolet−visible−near-infrared (UV−Vis−NIR) spectrophotometer (PE Lambda 750) with an integrating sphere and $BaSO_4$ as the baseline reference. A Fourier transform infrared spectrometer (Nicolet IS50, Thermo Fisher Scientific) with a gold integrating sphere was used to measure the second range with an optical glass as the baseline reference. The average reflectivity ($\overline{R}_{sun}$) in the solar spectral range was calculated using eq E1. The average transmission ($\overline{E}_{TIR}$) of the sample was calculated using eq E2.

$$\overline{R}_{sun} = \frac{\int_{300nm}^{2500nm} I_{sun}(\lambda) R_{sun}(\lambda) d\lambda}{\int_{300nm}^{2500nm} I_{sun}(\lambda) d\lambda} \quad \text{(E1)}$$

where λ is the wavelength, $R(\lambda)$ is the sample surface's reflectance spectra, and I_{sun} (λ) is the AM 1.5 solar spectral radiation defined by ISO standard 9845-1 (1992).

$$\overline{E}_{TIR} = \frac{\int_{8\mu m}^{13\mu m} I_B(\lambda, T)(1 - R_{TIR}(\lambda)) d\lambda}{\int_{8\mu m}^{13\mu m} I_B(\lambda, T) d\lambda} \quad \text{(E2)}$$

$$I_B(\lambda, T) = \frac{2hc^2}{\lambda^5 (e^{hc/\lambda K_B T} - 1)} \quad \text{(E3)}$$

where R_{TIR} (λ) is the film surface's reflectance in the thermal infrared spectrum. The emissivity spectrum was obtained by measuring the reflectivity (R_{TIR}), which was calculated using eq E2, in which transmittance can be ignored (it follows Kirchhoff's law of thermal radiation states). I_B (λ,T) is the blackbody radiation at temperature (T) according to Planck's

https://doi.org/10.1021/acsomega.2c01947
ACS Omega 2022, 7, 15247−15257

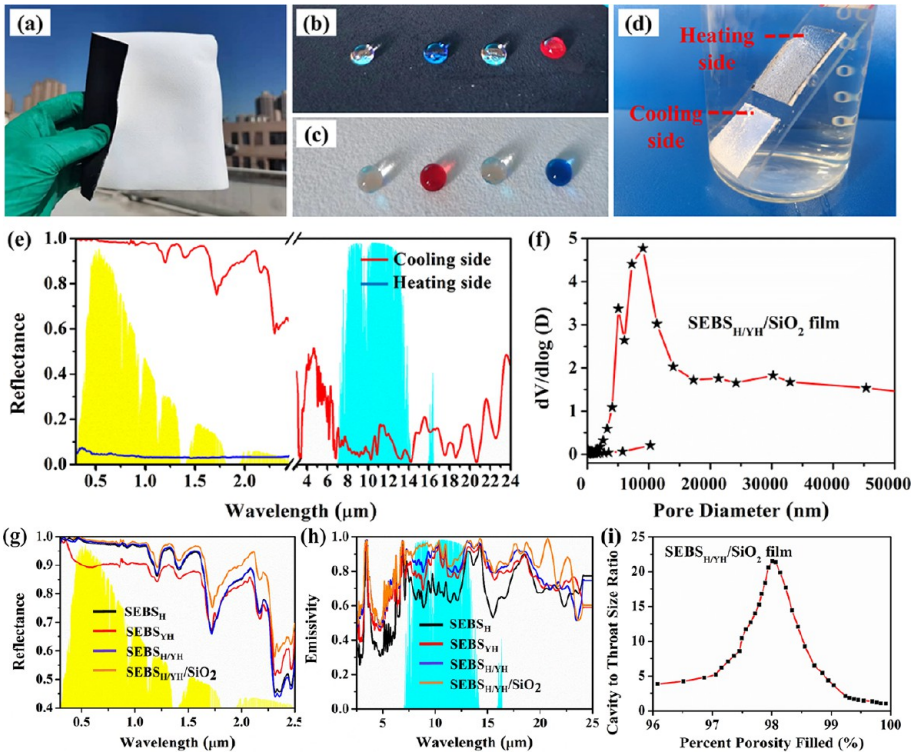

Figure 3. Optical and superhydrophobic properties of the CNT/PDMS-SEBS$_{H/YH}$/SiO$_2$ film. (a) Photograph of the film; (b, c) photograph of stained water droplets on the black side and white side of the film; (d) photograph of the film stuck to a glass slide in water; (e) reflectance spectra of the film with a thickness of 1020 μm at the AM1.5 spectra (yellow-shaded area) and an atmospheric transparency window (blue-shaded area) with the red color curve for the white side and the blue color curve for the black side; (f) statistical distribution of the pore diameters of the SEBS$_{H/YH}$/SiO$_2$ film. (g) Reflectance spectra of SEBS$_H$, SEBS$_{YH}$, SEBS$_{H/YH}$, and SEBS$_{H/YH}$/SiO$_2$ films; (h) emissivity spectra of SEBS$_H$, SEBS$_{YH}$, SEBS$_{H/YH}$, and SEBS$_{H/YH}$/SiO$_2$ films; (i) porosity of the SEBS$_{H/YH}$/SiO$_2$ film.

law (eq E3), where c is the speed of light, λ is the wavelength, h is Planck's constant, and K_B is the Boltzmann constant.

2.4.3. Cooling and Heating Performance Measurement. A self-made device was designed to measure the cooling and heating performance of the obtained dual-mode film. The film was placed, covering a 5 × 5 × 1 cm air cavity in a polystyrene foam wrapped with a layer of aluminum foil for reflecting sunlight to reduce solar heating. The apparatus was placed on a 1 m-high desk to reduce the influence of heat radiation from the rooftop heated by the sun. Furthermore, an infrared transparency polyethylene film (PE, 0.04 mm in thickness) was used to seal an air space above the setup to shield against convection and conduction with the environment. A four-channel K thermocouple (Yili Technology Co., Ltd., China) was used to detect the real-time temperature. The ambient air temperature around the sample was also tested. In addition, the solar irradiance and relative humidity were recorded by a data logging solar power meter (TES-132) and hygrothermograph (TH10R) around the device at the same time. The infrared images were taken by a thermal infrared camera (E6390). The indoor test device is smaller than that for outdoors, which has the same design concept and test method. A xenon lamp (Zhongjiao Jinyuan HXF300) with a high power that matches well with the solar spectrum was used to simulate solar radiation.

3. RESULTS AND DISCUSSION

3.1. Morphologies of the CNT/PDMS-SEBS$_{H/YH}$/SiO$_2$ Film. The structures both inside and on the surface of the film are very important to obtain cooling and superhydrophobic properties. In the preparation process, a phase separation method[30−32] was adopted to adjust the microstructure of the film. It was found that the ratio of S to EB in SEBS influenced greatly the morphology of the SEBS film, although they have the same chemical structures (Figure S1). The SEBS$_H$ film consists of spheres of about 2 μm on the surface, while SEBS$_{YH}$ has pores of about 5 μm with smooth walls (Figure 2a,b). When SEBS$_H$ and SEBS$_{YH}$ were mixed together, the obtained SEBS$_{H/YH}$ film consists of microscale pores with microscale particles decorated by spheres of about 2 μm, making the surface rough and hydrophobic with a CA of 135° (Figure 2c). When hydrophobic nanoparticles of SiO$_2$ were further incorporated, the as-obtained SEBS$_{H/YH}$/SiO$_2$ film possessed microspheres decorated with nanoparticles of SiO$_2$, forming a typical micro/nanostructured surface and making the film show a CA of 162° (Figure 2d and Figure S2). The SiO$_2$ roughened surface of the SEBS$_{H/YH}$/SiO$_2$ film might help enhance the scattering of solar light.

To obtain a dual-mode film, CNT/PDMS coating was made on one side of the SEBS$_{H/YH}$/SiO$_2$ film. The cross-sectional SEM image of the CNT/PDMS-SEBS$_{H/YH}$/SiO$_2$ film clearly depicted that the thickness of the film was about 1510 μm (Figure 2f), in which the CNT/PDMS coating was about 10 μm. The SEBS$_{H/YH}$/SiO$_2$ side was porous in its interior with abundant microscale spheres and SiO$_2$ aggregation (Figure 2e), which provides space for air to stay inside the film, favoring the enhancement of emissivity. The CNT/PDMS side was full of entangled nanowires of CNTs, roughening the coating surface (Figure 2g). The rough nanostructured surface in combination with the low surface energy substance of

https://doi.org/10.1021/acsomega.2c01947
ACS Omega 2022, 7, 15247−15257

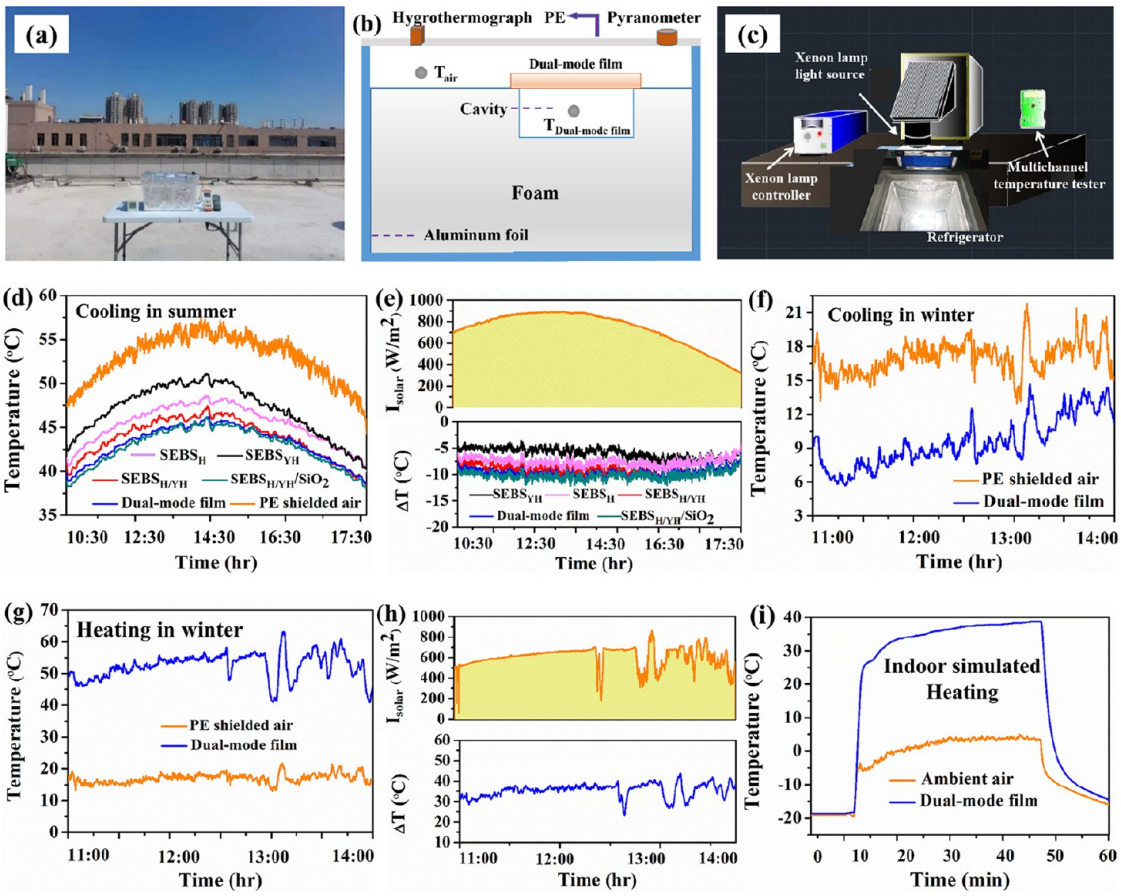

Figure 4. Cooling and heating performance of the dual-mode film. (a) Picture of the device on the rooftop; (b) schematic of the device for testing the cooling and heating performance; (c) diagram of the indoor-simulated heating device; (d) temperature tracking of air and the films in summer; (e) solar intensity and the temperature drop (ΔT) of panel (d); (f) temperature tracking of the air and dual-mode film in winter; (g) outdoor heating temperature profiles of the dual-mode film and ambient air; (h) solar intensity and the temperature rise (ΔT) in panel (g); (i) temperature tracking of the air and dual-mode film under indoor-simulated heating.

PDMS made the film at a mass ratio of CNT:PDMS = 1:2 superhydrophobic with a CA of 165° (Figure S3).

3.2. Superhydrophobic and Optical Properties of the Dual-Mode Film. The superhydrophobic surface usually has a water droplet contact angle of greater than 150° and the rolling angle of less than 10°. Water droplets are easy to roll on such a surface and take away the stains during the rolling process. The micro/nanorough structure and low surface energy property are two necessary conditions for constructing a superhydrophobic surface. The CNT/PDMS-$SEBS_{H/YH}/SiO_2$ film has two sides with contrast colors (Figure 3a), on both of which the stained water droplets exhibited spherical shapes, showing excellent liquid repellency (Figure 3b,c). When the film was dipped into water, a bright plastron formed on the surface because of the trapped air layer reflecting incident light (Figure 3d). When water droplets were put on the film surface, they rolled off easily (Movie 1). The black color of the other side was due to the full absorption of the visible spectrum of CNT in the CNT/PDMS coating, which only had an average reflectance of 2% in the 0.3−2.5 μm wavelength range. The white side consists of $SEBS_{H/YH}/SiO_2$, which is porous inside and rough on the surface, causing strong scattering of visible light and giving an ultrawhite appearance, which is ascribed to the mismatch of the refractive index between the air inside the pores, SiO_2 particles, and the $SEBS_{H/YH}$ copolymers. Calculation showed that the porous side of $SEBS_{H/YH}/SiO_2$ on a 1021 μm-thick film at a mass ratio of $SEBS_H$:$SEBS_{YH}$ = 6:4 (Figure S4) possesses a reflectance of 94% in the solar spectral region and an emissivity of 92% (Figure 3e). It was because of the finding that the film consists of rich micro/nanopores and microspheres in the 0.2−20 μm range (Figure 3f) with a percent porosity of 98% (Figure 3i), favoring scattering sunlight and emitting heat.[33−35]

For comparison, the emissivity and reflectance of the films of $SEBS_H$, $SEBS_{YH}$, $SEBS_{H/YH}$, and $SEBS_{H/YH}/SiO_2$ were also investigated. Calculations from Figure 3g showed that the $SEBS_{YH}$ film presents a lower average solar reflectance of 88% in the UV−Vis−NIR wavelengths because it consists only of large micropores in the range of 5−10 μm (Figure 2b), whereas the $SEBS_H$, $SEBS_{H/YH}$, and $SEBS_{H/YH}/SiO_2$ films exhibit high reflectance values of 91, 91, and 94%, respectively, because they consist of not only microscale pores but also microscale spheres, which scatter sunlight effectively.[36,37] Additionally, it was found that addition of SiO_2 made a positive effect on improving the reflectivity (Figure 3g). The emission spectra show that the SEBS-based film displays high emissivity. From Figure 3h, the average emissivity values of the films of $SEBS_H$, $SEBS_{YH}$, $SEBS_{H/YH}$, and $SEBS_{H/YH}/SiO_2$ were calculated to be 68, 82, 87, and 92%, respectively, in which the $SEBS_{H/YH}/SiO_2$ film shows the highest emissivity in the LWIR transparency window. It was obviously demonstrated that not only incorporation of the micro/nanoporous structure

https://doi.org/10.1021/acsomega.2c01947
ACS Omega 2022, 7, 15247−15257

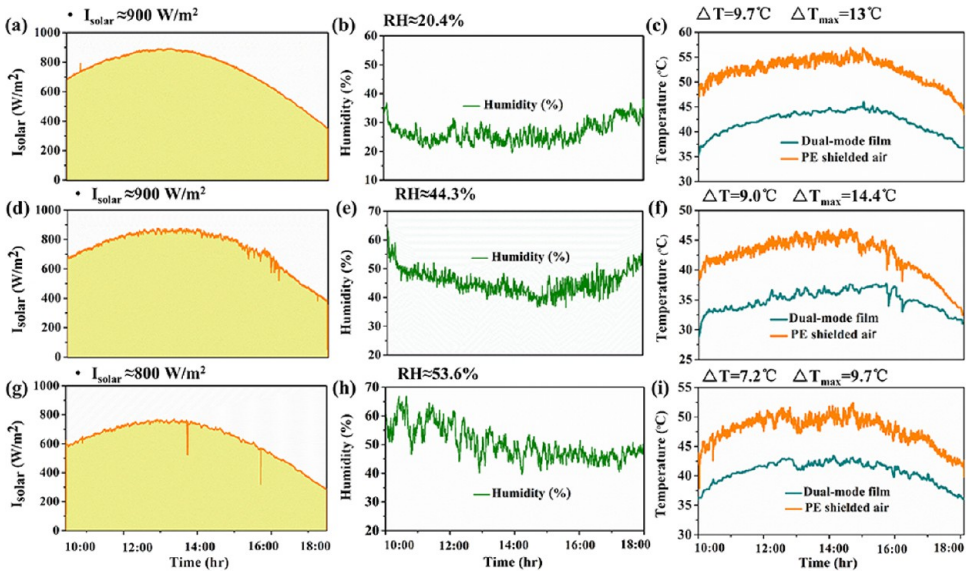

Figure 5. Cooling performance in various humidities and light intensities. (a−c) Solar irradiance, relative humidity, and temperatures of the ambient air and dual-mode film on a sunny day. (d−f) Solar irradiance, relative humidity, and temperatures of the ambient air and dual-mode film on a sunny day. (g−i) Solar irradiance, relative humidity, and temperatures of the ambient air and dual-mode film on a cloudy day.

enhanced the emissivity[38,39] but also adding SiO_2 due to the existence of a Si−O bond.[40,41]

3.3. Cooling and Heating Performance of the Dual-Mode Film. The radiative cooling performances of the films with a thickness of ∼1050 μm and a dimension of 9 cm × 9 cm were measured on the rooftop of a building under a clear and breeze sky in Xi'an (108.97°E, 34.38°N, Shaanxi, China) using a self-made setup (Figure 4a,b). It was found that both the $SEBS_H$ film and the $SEBS_{YH}$ film show a cooling ability, obtaining lower temperatures than the PE-shielded air (Figure 4d), indicating that SEBS is suitable to be a candidate for radiative materials. When $SEBS_H$ and $SEBS_{YH}$ were mixed together, the temperature obtained by $SEBS_{H/YH}$ was further decreased, which might be caused by the strengthened reflectance and the enhanced emittance due to the micro/nanostructure in the $SEBS_{H/YH}$ film as mentioned in Figure 2d. Additionally, when SiO_2 nanoparticles were incorporated, the obtained $SEBS_{H/YH}/SiO_2$ film displayed a further decreased temperature, which might be resulted from the enhanced emissivity by a Si−O bond in SiO_2. Figure 4e shows that, compared with the temperature around the film under a PE cover in the daytime with an average solar intensity (I_{solar}) of 900 W/m^2, the $SEBS_H$, $SEBS_{YH}$, $SEBS_{H/YH}$, and $SEBS_{H/YH}/SiO_2$ films got temperature drops ΔT of 6.7, 5.5, 8.3, and 11.3 °C, respectively, showing obviously increased cooling performance, which is in accordance with their reflectivity and emissivity mentioned above.

To fabricate a dual-mode film, the $SEBS_{H/YH}/SiO_2$ film was coated with CNT/PDMS. Excitedly, the obtained CNT/PDMS-$SEBS_{H/YH}/SiO_2$ film with the white side facing outside maintained excellent cooling ability with an average temperature drop ΔT of 11 °C similar to that of $SEBS_{H/YH}/SiO_2$, which indicates that coating of CNT/PDMS affected slightly the cooling ability of the $SEBS_{H/YH}/SiO_2$ film. The nocturnal radiation capacity measured by the same setup displayed an average temperature drop ΔT of 3 °C (Figure S5), showing cooling ability in nighttime. When the CNT/PDMS-$SEBS_{H/YH}/SiO_2$ film was directly exposed with the white side facing the ambient air without any convection shielding in daytime, it got a temperature drop ΔT of 7 °C (Figure S6). When using a xenon lamp as a standard solar light with irradiation of I_{solar} ≈ 1000 W/m^2 indoor, the dual-mode film can also achieve a temperature drop ΔT of 10 °C (Figure S7). These results demonstrated that the CNT/PDMS-$SEBS_{H/YH}/SiO_2$ film with the white side facing out works in the cooling mode, which could be applied in hot weather such as summer. Additionally, to better express the cooling effect of the film, we calculated the theory radiative cooling power of the dual-mode film (Figure S8), the power of average solar radiation is set to approximately 837.59 W/m^2, and the ambient temperature T_{amb} is assumed to be 312.15 K. The calculated maximum net cooling power is 99.8 W/m^2 at thermal equilibrium, which intuitively reflects excellent abilities of the dual-mode film for energy saving in summer.

However, when the CNT/PDMS-$SEBS_{H/YH}/SiO_2$ film was applied in winter with the white side facing out, it still achieved a temperature drop ΔT over 6 °C (Figure 4f) under I_{solar} ≈ 700 W/m^2 (Figure S9). Such cooling in cold weather goes against energy saving because it might cause extra energy consumption in heating for warming. In fact, outdoor application with the black coating of CNT/PDMS facing outside in cold weather was the design intention of the film, which works in heating mode. When the film was applied in heating mode in a simulated cold environment (−20 °C) under a xenon lamp with irradiation of I_{solar} ≈ 1000 W/m^2 (Figure 4c), its temperature was much higher than that of the surrounding air with a temperature rise ΔT of ∼40 °C (Figure 4i). Practical application in winter under an average I_{solar} of 700 W/m^2 (Figure 4h) showed that the temperature of the air covered by the film is much higher than that of the PE-shielded air with a temperature rise ΔT of 35.6 °C (Figure 4g), demonstrating excellent heating performance in cold weather. The integration of CNT/PDMS coating with $SEBS_{H/YH}/SiO_2$ into one film, namely, forming CNT/PDMS-$SEBS_{H/YH}/SiO_2$, obtained a material with two modes, which cools in summer and heats in winter.

To further evaluate and analyze the effects of the environment on the radiative cooling performance of the

https://doi.org/10.1021/acsomega.2c01947
ACS Omega 2022, 7, 15247−15257

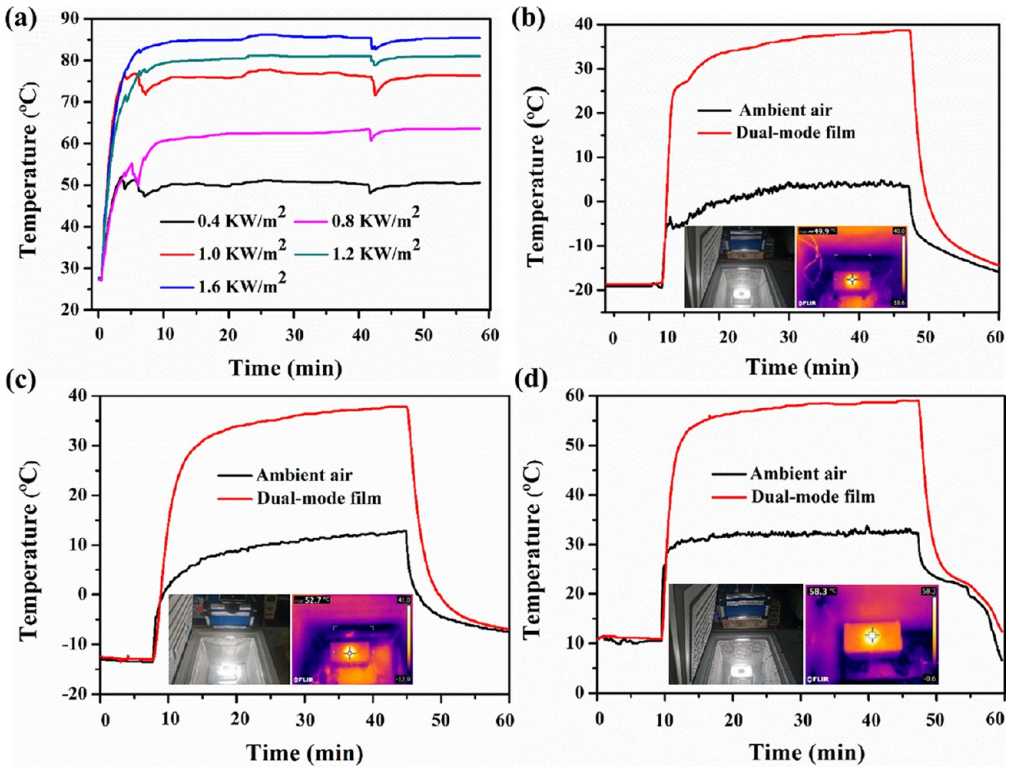

Figure 6. Solar heating performance of the dual-mode film in various cold environments provided by a refrigerator. (a) Temperature profiles of the film with irradiation time under different solar intensities when the refrigerator was set at 22 °C. Temperature profiles of the film and air close to the film when the refrigerator was set at (b) −20 °C, (c) −10 °C, and (d) 10 °C under irradiation of 1 kW/m^2.

dual-mode film, measurements were conducted about the temperature changes under different light intensities with different humidities. On a sunny day with a light intensity of up to ∼900 W/m^2 (Figure 5a), when the setup was placed on the rooftop with a surrounding humidity of ∼20.4% (Figure 5b), the temperature drop was 9.7 °C on average (Figure 5c); when the setup was placed on the lawn with a surrounding humidity of ∼44.3%, the temperature drop was 9.0 °C on average (Figure 5d−f). On a cloudy day with a light intensity of up to ∼700 W/m^2 (Figure 5g), when the setup was placed on the rooftop with a surrounding humidity of 53.6% (Figure 5h), the average temperature drop was 7.2 °C (Figure 5i). It is obvious that the cooling capacity of the film depends on the air humidity and the supply of solar light, which is in accordance with a previous report.[42]

To further investigate the heating performance of the dual-mode film, the setup was placed inside a refrigerator with different temperatures under different irradiation intensities. Figure 6a shows that irradiation of light increased quickly the temperature of the cavity covered by the film to a steady state in 5 min when the inside temperature of the refrigerator was set at 22 °C. Also, the steady temperature of the film increased with the increase in light intensity. Under a light intensity of 1 kW/m^2, the temperature underneath the film reached up to 75 °C. When the refrigerator was set at −20 °C, irradiation of the film obtained a temperature rise ΔT of about 40 °C (Figure 6b). When the refrigerator was set at −10 or 10 °C, the temperature rise was about 30 °C (Figure 6c,d). Infrared measurements under the simulated solar irradiance also confirmed the great heating capability of the dual-mode film (insets in Figure 6b−d). It was obviously shown that this dual-mode film could work for heating in winter.

3.4. Practical Applications of the Dual-Mode Film for the Shutter and Model Car. To demonstrate both the radiative cooling capability and solar heating capability of the dual-mode film on real objects, the film was applied in a self-made shutter as the blades. Infrared pictures were used to show the temperature difference between the film and the ambient air when the film was rotated clockwise to different angles. It was found that, when the blades were put at angles of 0°, 30°, 90°, 120°, and 180°, respectively (Figure 7a−e), the temperature of the blades increased correspondingly (Figure 7a$_1$−e$_1$). When the blades were set at 0° with the white side facing up (Figure 7a), the temperature under the blades was much lower than that of the ambient air (Figure 7f). The film worked in the typical cooling mode, obtaining a temperature drop of about 15 °C (Figure 7g). When the blades were rotated 30°, the temperature was gradually increased but still below the ambient temperature, indicating the cooling effect of the film. When the blades were rotated 120°, the temperature was increased gradually over the ambient temperature, showing a heating effect. At the angle of 180°, all the blades covered the whole surface above the shutter with the black side facing up and the temperature was much higher than that of the ambient air.

The film worked in the typical heating mode, obtaining a temperature rise of about 20 °C (Figure 7g). In addition, three identical car models were placed on the floor with one naked, one covered with a dual-mode film, and another covered by a commercial cooling material, which consisted of a thin plastic layer covered with aluminum foil (Figure 7h). The infrared images showed that the dual-mode film temperature was cooler than that of the commercial material and much cooler than that of the naked car model (Figure 7i). Figure 7j shows that

https://doi.org/10.1021/acsomega.2c01947
ACS Omega 2022, 7, 15247−15257

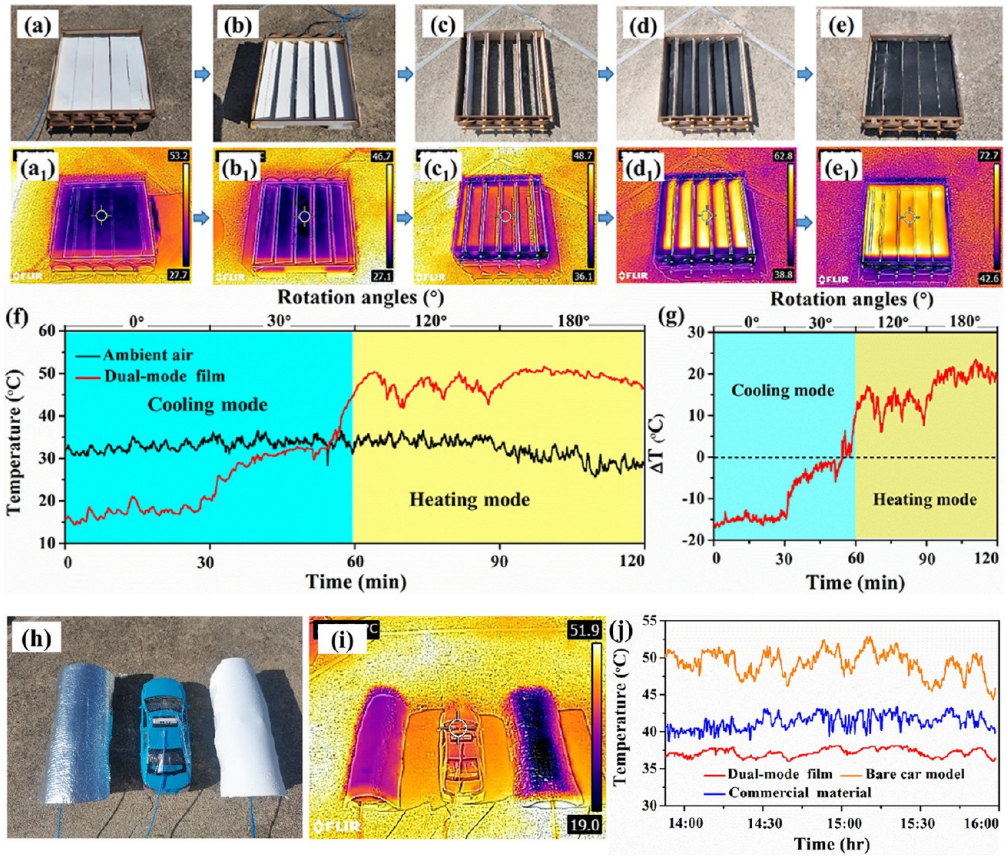

Figure 7. Practical applications of the dual-mode film. (a−e) Picture of the dual-mode film applied to a shutter and pictures of the blade rotated 0°, 30°, 90°, 120°, and 180°, respectively. (a_1−e_1) Infrared images of the shutter with the dual-mode film corresponding to panels (a)−(e). (f) Temperature profiles of 120 min inside the shutter with the blades at 0°, 30°, 120°, and 180°. (g) Temperature difference corresponding to panel (f). (h−j) Pictures, infrared images, and temperature profiles of the dual-mode film and commercial cooling material used for car model cooling.

the average temperatures on the surface of the bare car, underneath the commercial material, and underneath the dual-mode film were 49.3, 42.3, and 36.9 °C, respectively, indicating that the dual-mode film possesses greater cooling ability than the commercial material.

3.5. Self-Cleaning and Durability Performance of the Dual-Mode Film. As a material for outdoor applications, its surface inevitably suffers from the rain flushing and dust settling, which might affect the optical property and weaken the cooling performance as well as the heating ability. Inspiringly, the dual-mode film possesses unique superhydrophobicity on both sides, which makes the stains on the film easily taken away by water droplets (Figure 8a,b and Movie 2). Further, the cooling abilities of the film were evaluated before staining and after self-cleaning of the stains. The result shows that the self-cleaning effect of the white surface made the stains easily removed away and maintained the cooling function with a temperature drop ΔT of 10 °C, which is close to the original film with a drop ΔT of 11 °C (Figure 8c). Similarly, the superhydrophobic self-cleaning defends the black side from stain contamination and maintains the heating ability with a temperature rise by 35 °C, which is close to the original surface with a rise by 35.6 °C (Figure 8d). This shows the importance of making the film have superhydrophobicity, which favors long-time outdoor applications of the dual-mode film.

Additionally, the durability of self-cleaning was evaluated by immersion of the samples in solutions with different pH values for 5 days (Figure S10). It was found that the CAs were more than 150° and SAs were less than 10° on both sides of the dual-mode film after immersion. Also, the cooling and heating abilities changed slightly. The thermal stability of the film was tested by thermogravimetric analysis (Figure S11). It was found that the dual mode film can sustain the temperature of about 350 °C, exhibiting good thermal stability. This provides an effective guarantee for the long-term outdoor application of the dual-mode film.

4. CONCLUSIONS

A superhydrophobic dual-mode film was fabricated by phase separation of $SEBS_{H/YH}/SiO_2$ dispersion followed by CNT/PDMS coating. The film consists of a porous white side of $SEBS_{H/YH}/SiO_2$ with strong solar reflectivity and heat emissivity and a black side of CNT/PDMS with high solar absorptivity. The white side enables the film to cool objects in hot summer and the black side enables the film to heat objects in cold winter. The superhydrophobicity of the film protected the surface from contamination and endowed the film with sustainable cooling and heating performance. Also, the two modes of the film have been successfully demonstrated to be easily switched by a smart shutter through deliberate design, allowing a wide range of radiative cooling and solar heating systems to be constructed with cooling and heating abilities. We proposed that the integration design provides a way to achieve synergistic multifunction and will unleash the immense

https://doi.org/10.1021/acsomega.2c01947
ACS Omega 2022, 7, 15247−15257

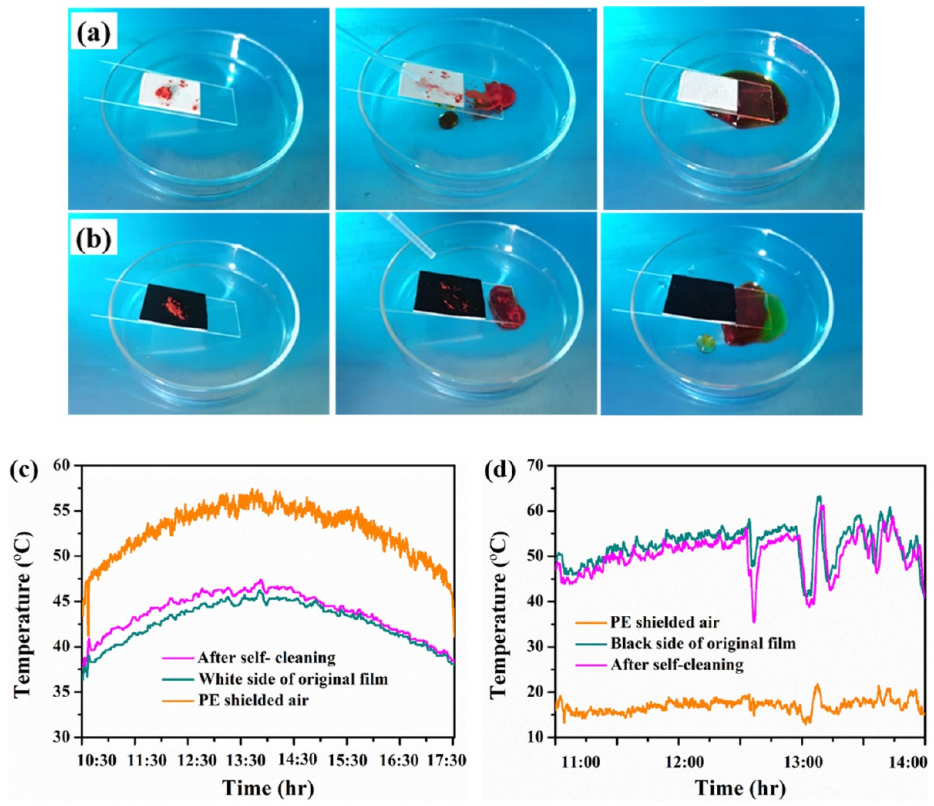

Figure 8. Self-cleaning performance of the dual-mode film. (a) Self-cleaning test for the white side. (b) Self-cleaning test for the black side. (c) Temperature profiles of the white side of the film before and after the self-cleaning test and the PE-shielded air. (d) Temperature profiles of the black side of the film before and after the self-cleaning test and the PE-shielded air.

potential for modern intelligent home in energy saving and sustainable cooling and heating indoor.

■ ASSOCIATED CONTENT

Supporting Information

The Supporting Information is available free of charge at https://pubs.acs.org/doi/10.1021/acsomega.2c01947.

Chemical structure of SEBS; effect of SiO_2 content on film reflectivity and contact angle; effects of proportion of PDMS and CNT on the superhydrophobicity of the CNT/PDMS-$SEBS_{H/YH}$/SiO_2 film; effects of the composite ratio of $SEBS_H$ to $SEBS_{YH}$ and thickness on the reflectance of the $SEBS_{H/YH}$ film; nighttime cooling measurement; daytime cooling measurement without a PE cover; indoor-simulated temperature drop measurement; theoretical calculations of the radiation cooling power of the dual-mode film without a PE cover; winter cooling measurement; self-cleaning durability of the dual-mode film; thermal stability of the dual-mode film (PDF)

Superhydrophobic properties of the dual-mode film (MP4)

Anticontamination and self-cleaning properties of the dual-mode film (MP4)

■ AUTHOR INFORMATION

Corresponding Authors

Chao-Hua Xue − *College of Chemistry and Chemical Engineering and College of Bioresources Chemical and Materials Engineering, Shaanxi University of Science and Technology, Xi'an 710021, China*; orcid.org/0000-0001-6780-8387; Email: xuechaohua@126.com

Xiao-Jing Guo − *College of Materials Science and Engineering, Shaanxi University of Science and Technology, Xi'an 710021, China*; Email: guoxiaojing2015@126.com

Authors

Jiang-He Wang − *College of Chemistry and Chemical Engineering, Shaanxi University of Science and Technology, Xi'an 710021, China*

Bing-Ying Liu − *College of Environmental Science and Engineering, Shaanxi University of Science and Technology, Xi'an 710021, China*

Li-Cui Hu − *College of Bioresources Chemical and Materials Engineering, Shaanxi University of Science and Technology, Xi'an 710021, China*

Hui-Di Wang − *College of Materials Science and Engineering, Shaanxi University of Science and Technology, Xi'an 710021, China*

Fu-Quan Deng − *College of Bioresources Chemical and Materials Engineering, Shaanxi University of Science and Technology, Xi'an 710021, China*

Complete contact information is available at: https://pubs.acs.org/10.1021/acsomega.2c01947

Notes

The authors declare no competing financial interest.

■ ACKNOWLEDGMENTS

This work was supported by the National Natural Science Foundation of China (52103263), the Natural Science

Foundation of Shaanxi Province (2020JM-506), China Postdoctoral Science Foundation (2020M683410), and a major project of Ministry of Science and Technology of China (2017YFB0307700).

REFERENCES

(1) Yin, X.; Yang, R.; Tan, G.; Fan, S. Terrestrial Radiative Cooling: Using the Cold Universe as a Renewable and Sustainable Energy Source. *Science* **2020**, *370*, 786−791.
(2) Raman, A. P.; Anoma, M. A.; Zhu, L.; Rephaeli, E.; Fan, S. Passive Radiative Cooling below Ambient Air Temperature under Direct Sunlight. *Nature* **2014**, *515*, 540−544.
(3) Li, Z.; Chen, Q.; Song, Y.; Zhu, B.; Zhu, J. Fundamentals, Materials, and Applications for Daytime Radiative Cooling. *Adv. Mater. Technol.* **2020**, *5*, 1901007.
(4) Zhao, B.; Hu, M.; Ao, X.; Chen, N.; Pei, G. Radiative cooling: A Review of Fundamentals, Materials, Applications, and Prospects. *Appl. Energy* **2019**, *236*, 489−513.
(5) Wang, H.-D.; Xue, C.-H.; Guo, X.-J.; Liu, B.-Y.; Ji, Z.-Y.; Huang, M.-C.; Jia, S.-T. Superhydrophobic Porous Film for Daytime Radiative Cooling. *Appl. Mater. Today* **2021**, *24*, 101100.
(6) Liu, B. Y.; Xue, C. H.; Zhong, H. M.; Guo, X. J.; Wang, H. D.; Li, H. G.; Du, M. M.; Huang, M. C.; Wei, R. X.; Song, L. G.; Chang, B.; Wang, Z. Multi-Bioinspired Self-Cleaning Energy-Free Cooling Coatings. *J. Mater. Chem. A* **2021**, *9*, 24276−24282.
(7) Wang, T.; Wu, Y.; Shi, L.; Hu, X.; Chen, M.; Wu, L. A Structural Polymer for Highly Efficient All-day Passive Radiative Cooling. *Nat. Commun.* **2021**, *12*, 365.
(8) Xiao, R.; Hou, C.; Yang, W.; Su, Y.; Li, Y.; Zhang, Q.; Gao, P.; Wang, H. Infrared-Radiation-Enhanced Nanofiber Membrane for Sky Radiative Cooling of the Human Body. *ACS Appl. Mater. Interfaces* **2019**, *11*, 44673−44681.
(9) Yang, Z.; Sun, H.; Xi, Y.; Qi, Y.; Mao, Z.; Wang, P.; Zhang, J. Bio-Inspired Structure Using Random, Three-Dimensional Pores in the Polymeric Matrix for Daytime Radiative Cooling. *Sol. Energy Mater. Sol. Cells* **2021**, *227*, No. 111101.
(10) Yang, M.; Zou, W.; Guo, J.; Qian, Z.; Luo, H.; Yang, S.; Zhao, N.; Pattelli, L.; Xu, J.; Wiersma, D. S. Bioinspired "Skin" with Cooperative Thermo-Optical Effect for Daytime Radiative Cooling. *ACS Appl. Mater. Interfaces* **2020**, *12*, 25286−25293.
(11) Ge, D.; Lee, E.; Yang, L.; Cho, Y.; Li, M.; Gianola, D. S.; Yang, S. A Robust Smart Window: Reversibly Switching from High Transparency to Angle-Independent Structural Color Display. *Adv. Mater.* **2015**, *27*, 2489−2495.
(12) Kim, H. N.; Ge, D.; Lee, E.; Yang, S. Multistate and On-Demand Smart Windows. *Adv. Mater.* **2018**, *30*, 1803847.
(13) Xu, J.; Zhang, Y.; Zhai, T.-T.; Kuang, Z.; Li, J.; Wang, Y.; Gao, Z.; Song, Y.-Y.; Xia, X. Electrochromic-Tuned Plasmonics for Photothermal Sterile Window. *ACS Nano* **2018**, *12*, 6895−6903.
(14) Zhang, Y.; Tso, C. Y.; Iñigo, J. S.; Liu, S.; Miyazaki, H.; Chao, C. Y. H.; Yu, K. M. Perovskite Thermochromic Smart Window: Advanced Optical Properties and Low Transition Temperature. *Appl. Energy* **2019**, *254*, No. 113690.
(15) Zhou, Y.; Wang, S.; Peng, J.; Tan, Y.; Li, C.; Boey, F. Y. C.; Long, Y. Liquid Thermo-Responsive Smart Window Derived from Hydrogel. *Joule* **2020**, *4*, 2458−2474.
(16) Li, X.; Sun, B.; Sui, C.; Nandi, A.; Fang, H.; Peng, Y.; Tan, G.; Hsu, P. C. Integration of Daytime Radiative Cooling and Solar Heating for Year-Round Energy Saving in Buildings. *Nat. Commun.* **2020**, *11*, 6101.
(17) Fang, H.; Xie, W.; Li, X.; Fan, K.; Lai, Y. T.; Sun, B.; Bai, S.; Padilla, W. J.; Hsu, P. C. A Triple-Mode Midinfrared Modulator for Radiative Heat Management of Objects with Various Emissivity. *Nano Lett.* **2021**, *21*, 4106−4114.
(18) Kang, S. K.; Ho, D. H.; Lee, C. H.; Lim, H. S.; Cho, J. H. Actively Operable Thermoresponsive Smart Windows for Reducing Energy Consumption. *ACS Appl. Mater. Interfaces* **2020**, *12*, 33838−33845.
(19) Zhao, H.; Sun, Q.; Zhou, J.; Deng, X.; Cui, J. Switchable Cavitation in Silicone Coatings for Energy-Saving Cooling and Heating. *Adv. Mater.* **2020**, *32*, 2000870.
(20) Hsu, P. C.; Liu, C.; Song, A. Y.; Zhang, Z.; Peng, Y.; Xie, J.; Liu, K.; Wu, C. L.; Catrysse, P. B.; Cai, L.; Zhai, S.; Majumdar, A.; Fan, S.; Cui, Y. A Dual-Mode Textile for Human Body Radiative Heating and Cooling. *Sci. Adv.* **2017**, *3*, No. e1700895.
(21) Guo, X.-J.; Xue, C.-H.; Jia, S.-T.; Ma, J.-Z. Mechanically Durable Superamphiphobic Surfaces via Synergistic Hydrophobization and Fluorination. *Chem. Eng. J.* **2017**, *320*, 330−341.
(22) Guo, X.-J.; Xue, C.-H.; Li, M.; Li, X.; Ma, J.-Z. Fabrication of Robust, Superhydrophobic, Electrically conductive and UV-blocking fabrics via layer-by-layer assembly of carbon nanotubes. *RSC Adv.* **2017**, *7*, 25560−25565.
(23) Xue, C.-H.; Zhang, L.; Wei, P.; Jia, S.-T. Fabrication of Superhydrophobic Cotton Textiles with Flame Retardancy. *Cellulose* **2016**, *23*, 1471−1480.
(24) Xue, C.-H.; Li, X.; Jia, S.-T.; Guo, X.-J.; Li, M. Fabrication of Robust Superhydrophobic Fabrics Based on Coating with PVDF/PDMS. *RSC Adv.* **2016**, *6*, 84887−84892.
(25) Xue, C.-H.; Deng, L.-Y.; Jia, S.-T.; Wei, P.-B. Fabrication of Superhydrophobic Aromatic Cotton Fabrics. *RSC Adv.* **2016**, *6*, 107364−107369.
(26) Xue, C. H.; Bai, X.; Jia, S. T. Robust, Self-Healing Superhydrophobic Fabrics Prepared by One-Step Coating of PDMS and Octadecylamine. *Sci. Rep.* **2016**, *6*, 27262.
(27) Xue, C.-H.; Li, Y.-R.; Hou, J.-L.; Zhang, L.; Ma, J.-Z.; Jia, S.-T. Self-Roughened Superhydrophobic Coatings for Continuous Oil−Water Separation. *J. Mater. Chem. A* **2015**, *3*, 10248−10253.
(28) Xue, C.-H.; Guo, X.-J.; Ma, J.-Z.; Jia, S.-T. Fabrication of Robust and Antifouling Superhydrophobic Surfaces via Surface-Initiated Atom Transfer Radical Polymerization. *ACS Appl. Mater. Interfaces* **2015**, *7*, 8251−8259.
(29) Xue, C.-H.; Ji, P.-T.; Zhang, P.; Li, Y.-R.; Jia, S.-T. Fabrication of Superhydrophobic and Superoleophilic Textiles for Oil−Water Separation. *Appl. Surf. Sci.* **2013**, *284*, 464−471.
(30) Wang, F.; Altschuh, P.; Ratke, L.; Zhang, H.; Selzer, M.; Nestler, B. Progress Report on Phase Separation in Polymer Solutions. *Adv. Mater.* **2019**, *31*, 1806733.
(31) Yoshimoto, K.; Taniguchi, T. Viscoelastic Phase Separation Model for Ternary Polymer Solutions. *J. Chem. Phys.* **2021**, *154*, 104903.
(32) Cheng, B.; Zhao, H.; Yang, J.; Zhao, J. Continuous Evolution of the Re-Entrant Phase Separation in Evaporating Droplets of Polymer Solutions. *Polymer* **2021**, *237*, 124327.
(33) Wang, X.; Liu, X.; Li, Z.; Zhang, H.; Yang, Z.; Zhou, H.; Fan, T. Scalable Flexible Hybrid Membranes with Photonic Structures for Daytime Radiative Cooling. *Adv. Funct. Mater.* **2019**, *30*, 1907562.
(34) Bhatia, B.; Leroy, A.; Shen, Y.; Zhao, L.; Gianello, M.; Li, D.; Gu, T.; Hu, J.; Soljačić, M.; Wang, E. N. Passive Directional Sub-Ambient Daytime Radiative Cooling. *Nat. Commun.* **2018**, *9*, 5001.
(35) Kou, J.; Jurado, Z.; Chen, Z.; Fan, S.; Minnich, A. J. Daytime Radiative Cooling Using Near-Black Infrared Emitters. *ACS Photonics* **2017**, *4*, 626−630.
(36) Wang, B.; Zhao, C. Effect of Dependent Scattering on Light Absorption in Highly Scattering Random Media. *Int. J. Heat Mass Transfer* **2018**, *125*, 1069−1078.
(37) Michelle, A.; Visbal, O.; Raymond, L.; Konger, Y. L.; Kim, Y. L. Telecentric Suppression of Diffuse Light in Imaging of Highly Anisotropic Scattering Media. *Opt. Lett.* **2016**, *41*, 143−146.
(38) Zhang, H.; Ly, K. C. S.; Liu, X.; Chen, Z.; Max, Y.; Wu, Z.; Wang, X.; Zheng, Y.; Zhou, H.; Fan, T. Biologically Inspired Flexible Photonic Films for Efficient Passive Radiative Cooling. *Proc. Natl. Acad. Sci.* **2020**, *117*, 14657−14666.
(39) Wang, Z.; Yan, S.; Cui, H.-C.; Cheng, G.; Ma, H.; Zhang, Q.-M.; Zhang, Q.-P.; Liu, J.-M.; Tan, B.; Zhang, C. Porous Organic Polymer from Aggregation-Induced Emission Macrocycle for White-Light Emission. *Macromolecules* **2018**, *51*, 7863−7871.

https://doi.org/10.1021/acsomega.2c01947
ACS Omega 2022, 7, 15247−15257

(40) Queeney, K. T.; Herbots, N.; Shaw, J. M.; Atluri, V.; Chabal, Y. J. Infrared Spectroscopic Analysis of an Ordered Si/SiO_2 Interface. *Appl. Phys. Lett.* **2004**, *84*, 493−495.
(41) Li, D.; Liu, X.; Li, W.; Lin, Z.; Zhu, B.; Li, Z.; Li, J.; Li, B.; Fan, S.; Xie, J.; Zhu, J. Scalable and Hierarchically Designed Polymer Film as a Selective Thermal Emitter for High-performance All-day Radiative Cooling. *Nat. Nanotechnol.* **2021**, *16*, 153−158.
(42) Zhao, D.; Aili, A.; Zhai, Y.; Xu, S.; Tan, G.; Yin, X.; Yang, R. Radiative Sky Cooling: Fundamental Principles, Materials, and Applications. *Appl. Phys. Rev.* **2019**, *6*, No. 021306.

https://doi.org/10.1021/acsomega.2c01947
ACS Omega 2022, 7, 15247−15257